Research Article

Taj Munir*, Rana Atta ur Rahman, Ali Raza, Muhammad Yousaf Malik, Ilyas Khan, Ahmed Ashour, Abd Allah A. Mousa, and Ali Saeed Alqahtani

Multiple-scale analysis of the parametric-driven sine-Gordon equation with phase shifts

https://doi.org/10.1515/phys-2022-0041
received January 12, 2022; accepted April 12, 2022

Abstract: In this article, we model the current and voltage across the weak link between two superconductors. This gives us a nonhomogeneous, nonlinear parametric-driven sine-Gordon equation with phase shifts. This model equation cannot be solved directly but can be approximated. For the approximations, we use two methods, and analytic perturbation method and the numerical approximation method known as the Runge–Kutta method. For the analytic method, we construct a perturbation expansion method with multiple-scale expansion. We discuss the parametric-driven in the sine-Gordon equation with phase shifts for the 0–π–0 junction. Further, we also describe the breathing modes for various order of perturbation. At the end, we compare the solutions obtained via perturbation and numerical methods of parametric-driven sine-Gordon equation with phase shifts. Finally, we concluded that the modes of the breathing decay to a constant in both cases. Also we found a good agreement between both approximate methods.

Keywords: sine-Gordon equation, multiple-scale expansion, Josephson junction, 0–π–0 junction and Runge–Kutta method

1 Introduction

Brian David was a British physicist who established the mathematical relationships for the voltage and current across the weak link between two superconductors. This phenomenon of super current is called Josephson effect, and the device is known as Josephson junction (JJ). A weak link can possibly consist of superconductor nonsuperconducting superconductor metal (S–N–S) and superconductor insulator superconductor junction (S–I–S), or a physical constriction, which weakens the superconductivity at the point of contact. The S–I–S is shown in Figure 1. Extremely fast switch is one of the most important applications of Josephson effects and two Josephson contacts jointly can be used to measure the magnetic flux.

The compensation of radiation loses along with additional dissipative loses were studied by resonant drive of kink. The resonance taking place when natural wobbling frequency becomes equal to the driving frequency. The emission of second-harmonic radiation becomes a cause of decay of oscillations amplitude in freely wobbling kink given in Oxtoby and Barashenkov [1].

The Josephson Junction having regimes with the phase shift was originated by a rapidly oscillating AC-Drive. Furthermore, it is found that the critical length increases by $(0$–π–$0)$ junction of AC-drive given in Ali *et al.* [2]. The perturbed stochastic sine-Gordon equation has been solved for switching events from the superconducting meta-stable state, given in the study by Spagnolo *et al.* [3]. The following three cases were used for nonlinear relaxation dynamics:

* **Corresponding author: Taj Munir,** Abdus Salam School of Mathematical Sciences, Government College University Lahore, New Muslim town 68-B, Lahore 54600, Pakistan, e-mail: taj_math@hotmail.com
Rana Atta ur Rahman: University of Engineering and Technology, Taxila, Pakistan
Ali Raza: Abdus Salam School of Mathematical Sciences, Government College University Lahore, New Muslim town 68-B, Lahore 54600, Pakistan
Muhammad Yousaf Malik, Ali Saeed Alqahtani: Department of Mathematics, College of Sciences, King Khalid University, Abha 61413, Kingdom of Saudi Arabia
Ilyas Khan: Department of Mathematics, College of Science Al-Zulf, Majmaah University, Al-Majmaah 11952, Saudi Arabia, e-mail: i.said@mu.edu.sa
Ahmed Ashour: Engineering Mathematics and Physics Department, Faculty of Engineering and Technology, Future University in Egypt, New Cairo 11845, Egypt
Abd Allah A. Mousa: Department of Mathematics and Statistics, College of Science, Taif University, P.O. Box 11099, Taif 21944, Saudi Arabia

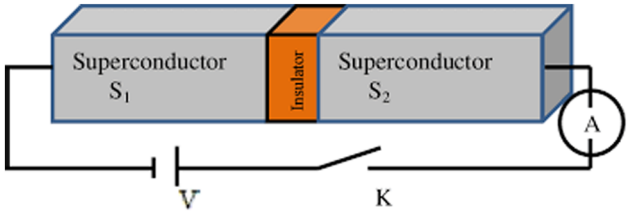

Figure 1: Josephson junction [CSIRO].

(i) Overlapped Josephson junction.
(ii) Graphene-based Josephson junction.
(iii) Electron in an N-Type GaAs crystal driven by fluctuated electric field.

They found the dependence of the trajectories of bubbles on the arrangement of main functional regions. This dependence was found to be an evidence of existence of the relation between DNA functioning and dynamics. The numerical simulations of Gross–Pitaevskii equations were performed to predict spatially localized and temporarily oscillating nonlinear excitation's. These results resemble with the solutions of sine-Gordon equation known as breather with a difference of slow decay has been explained in the study by Su *et al.* [4].

A new phenomenon was revealed for long-time resonant energy exchange in carbon nanotubes (CNTs) with radial breathing mode. It was found to be stable wide excitation energy range. The modified nonlinear Schrödinger equation (NLS) describes the nonlinear dynamics of CNTs given in Smirnov and Manevitch [5]. An initial value problem of Hamilton's principle applied to nonconservative systems, was proposed for complex partial differential equations of the NLS type equation. In the study by Rossi *et al.* [6], dynamics of coherent solitary wave structures of NCVA was examined, and also it is proved that the NLSr and linear perturbative variation equations are equivalent through nonconservative variation methods.

The dubbed oscillations built in the Minkowski background for some nonlinear potentials such as axionic sine-Gordon potential are a counterpart of the real scalar field. The bosonic fields with mass such as axions, axion-like candidates, and hidden photons. These fields form the breathing mode. The space–time geometry and the field oscillate can interact the cluster at the center of stars. In the study by Brito *et al.* [7], it was concluded that these stars are generically stable, and also the criteria for instability are provided. By using the sitter geometry, the stability of membranes was analyzed and found that the Jacobi equation specializes to a Klein–Gordon equation as explained in the study by Norma *et al.* [8].

The application of the magnetic field results in partially gaped spectrum, which is one of the main problems of Rashba spin–orbit coupling in nanowires such as helical gap, spectral function, structure factor, or the tunneling density of states. The form factors of emerging sine-Gordon model and besonization, a re-normalization group analysis, were used to calculate dynamic response functions. It was shown how two types of helical gaps, can be distinguished in experiments given in the study by Pedder *et al.* [11]. The nontrivial dynamics was expected associated with soliton lattice oscillations and breathing as per sine-Gordon equation. It is concluded that rich post-quench dynamics leads to thermalized and pre-thermalized stationery states that display strong dependence on the initial ground-state can be seen in the study by Yin and Radzihovsky [12].

The dynamics of a soliton in the generalized NLS with a small external potential ζV was studied by Bambusi and Maspero [13]. Energy of such a mechanical system for any positive integer r remains almost conserved up to an order of ζ^{-r} explained . It is possible to convert breather into different types of nonlinear stationery waves; W-shaped soliton, periodic wave, M-shaped soliton, and multipeak soliton. The nonlinear interactions between these waves display some novel patterns due to nonpropagating characteristics of solitons. It was concluded that transition occurs in the low perturbation frequency region at the modulational stability region, given in the study by Wang *et al.* [14].

The analytical and numerical solutions of direct-driven sine-Gordon (sG) equation modeled by the Josephen junction on a finite domain with π-discontinuous points characterized by a jump of π in the phase difference of the junction, which is known as 0–π–0 junction. A Hamiltonian energy character length has been used. It was shown that there is an instability in which semi fluxons are spontaneously generated. These semi fluxons depend on the length of the junction, the facet length, and the applied bias current explained in Ahmad *et al.* [15]. The size of the bounded domain plays an important role during occurrence of qualitative distinct phenomena in nonlinear dynamical system. The radiation emitted by bonded nonlinear waves were studied. The multimode dispersive waves were generated by spatio-temporal oscillations of solitons in multimode fibre.

The source of coherent electromagnetic waves was investigated with unprecedented spectral range given in the study by Wright *et al.* [16]. The spatio-temporal non-homogeneous direct drive type sine-Gordon equation with phase shift and a double-well potential was considered. An interested study of the closely related model to our current work of sine-Gordon equation with phase shift was explained by Ali *et al.* [17]. They also used multiple-scale expansion with the perturbation method. It was founded that the algebraic mode decay from discrete to continuous spectrum. In the paper they considered the direct driven vase, while ours is the parameter with extra phase shift.

The radial breathing modes (RBMs) of CNTs is a low-frequency mode but used for the strongest features observed in the CNT Raman spectrum. The RBMs are modes of vibration characteristic of carbon nan-otubes, which do not appear in any other structure (beams, plates, or shells), see, for example, She *et al.* [18]. Further, the RBMs arise only in the presence of free-free boundary conditions (when the CNTs are left free to vibrate without constraints imposed on the edges), while they do not appear in other boundary conditions (simply supported and clamped), see, for example, Strozzi *et al.* [19]. Also, RBMs are studied experimentally by resonant Raman spectroscopy and numerically by molecular dynamics simulations, see, for example, Araujo *et al.* [20], Batra and Gupta [21], and Rehman *et al.* [9], and Ahmad [10].

In this article, we considered a parametric-driven sine-Gordon equation with two phase shifts $\theta(x)$ as well as with the driven frequency term $h\sin\Omega t$. This extra source term provides energy to the system. Further, we extend the previous work of Ali *et al.* [2] and study the decay rate of a localized modes of the trivial ground-state. For the solution, we used two approximate methods: a perturbation method together with multiple-scale expansion and a numerical method known as Runge–Kutta method of order four.

The outline of this work is given as follows: In Section 2, we introduce the mathematical formulation, the un-driven and driven cases, and the detail analytic calculation. While in Section 3, we derived an amplitude equation. The numerical computations are given in Section 4. In Section 5, we provide the results and discussion of this work. Finally, we present the conclusion and some future research work in Section 6. The mathematical derivation is presented in the Appendix section.

2 Mathematical formulation

In this article, we modeled a weak link between two superconductors and obtained the following in-homogeneous, nonlinear parametric-driven sine-Gordon equation with phase shifts. This is given as follows:

$$u_{xx} - u_{tt} = \sin(\theta(x) + u) + h\sin(\Omega t)\sin(\theta(x) + u). \quad (1)$$

This model is a non linear partial differential equation, which represents the infinitely long Josephson junction. Here, $\theta(x)$ is the phase shift, $h\sin(\Omega t)$ is a driving force, and $h > 0$ is the amplitude of the applied time periodic AC-drive. This is proportional to the applied microwave power with $h \sim O(\zeta^3)$. Here, ζ is the perturbed parameter. With this assumption, it will appear in the higher order of ζ. Also we use the perturbation method with multiple-scale expansion. The frequency is defined as $\Omega = \eta(1 + \rho)$ and $\Omega t = \eta\tau$. Here, Ω is a driving frequency and τ is the transform parameter. Equation (1) is dimensionless, t and x are normalized by λ_J, which is known as the Josephson penetration length. The η_p^{-1} is the inverse plasma frequency.

The unknown u, phase field is subjected to the continuity conditions at the position of the jump as follows:

$$u(\pm a) = u(\pm a),\ u_x(\pm a) = u_x(\pm a). \quad (2)$$

Here, a is the facet length. In this study, we take $0{-}\pi{-}0$ junction. So $-a$ is for the left junction and $+a$ for the right junction.

$$\theta(x) = \begin{cases} 0, & |x| > a \\ \pi, & |x| \le a. \end{cases} \quad (3)$$

Here, a is the facet length and $a < \pi/4$. In this work, we will study two cases of the internal phase shift. The initial conditions are given as follows:

$$u = U_0(x) + B_0U_1(x, 0), \quad u_t(x, 0) = 0. \quad (4)$$

Now we use the transformation in Eq. (1) and we obtained

$$u_{xx} - (1 + \rho)^2u_{\tau\tau} = \sin(\theta(x) + u) + h\sin(\eta\tau)\sin(\theta(x) + u). \quad (5)$$

The scaling parameters $h = \zeta^3H$ and $\rho = \zeta^3R$. Further, we expand equation (5) by using the perturbation method together with multiple-scale expansion. For this, u can be expanded as follows:

$$u = u_0 + \zeta u_1 + \zeta^2u_2 + \zeta^3u_3 + \zeta^4u_4 \ldots. \quad (6)$$

The multiple-scale spatial and temporal coordinates and their derivatives are given as follows:

$$X_n = \zeta^n x, \quad T_n = \zeta^n \tau, \quad \text{for } n = 0, 1, 2, 3 \ldots,$$

with

$$d_n = \frac{\partial}{\partial T_n}, \quad \partial_n = \frac{\partial}{\partial X_n} \quad \text{for } n = 0, 1, 2, 3 \ldots$$
$$\frac{\partial}{\partial x} = \partial_0 + \zeta\partial_1 + \zeta^2\partial_2 + \zeta^3\partial_3 + \ldots$$
$$\frac{\partial}{\partial \tau} = d_0 + \zeta d_1 + \zeta^2 d_2 + \zeta^3 d_3 + \ldots.$$

A special case, *i.e.*, for $h = 0$, the model Eq. (1) will give the following simplified sG-equation with phase shift as follows:

$$u_{xx} - u_{tt} = \sin(\theta(x) + u).$$

This case has been explained in the study by Ali *et al.* [2] and no need to repeat again.

2.1 Driven case of the model equation

In this work, our main focus is to study the parametric-driven case, *i.e.*, for $h \neq 0$ in Eq. (5). By substituting the scaling parameters and multiple-scale derivatives in Eq. (5), we obtain the different equation corresponding to the order of each ζ.

2.1.1 $O(1)$-equation

After expansion and comparison on both sides, we obtain the following equation at first order:

$$O(1) : \partial_0^2 u_0 - d_0^2 u_0 = \sin(\theta + u_0). \tag{7}$$

The ground-state solution, *i.e.*, $u_0 = 0$ for 0–π–0 junction satisfies Eq. (7).

2.1.2 $O(\zeta)$-equation

The equation at $O(\zeta)$ is given by

$$\begin{aligned} O(\zeta) : \partial_0^2 u_1 - d_0^2 u_1 - \cos(\theta + u_0)u_1 \\ = 2d_0 d_1 u_0 - \partial_0\partial_1 u_0. \end{aligned} \tag{8}$$

By substituting $u_0 = 0$ in (8), we obtained the following equation:

$$\partial_0^2 u_1 - d_0^2 u_1 - \cos\theta u_1 = 0. \tag{9}$$

The breather solution of the aforementioned equation is given by

$$u_1(X_0, T_0) = Ee^{i\eta T_0}\begin{cases} \cos(a\sqrt{1+\eta^2})e^{\sqrt{1-\eta^2}(a+X_0)} + c.c, & X_0 < -a, \\ \cos(X_0\sqrt{1+\eta^2}) + c.c & |X_0| \le a, \\ \cos(a\sqrt{1+\eta^2})e^{\sqrt{1-\eta^2}(a-X_0)} + c.c, & X_0 > a. \end{cases} \tag{10}$$

Here, $E = E(X_1, X_2 \ldots T_1, T_2 \ldots)$ is an amplitude of oscillation.

2.1.3 $O(\zeta^2)$-equations

We obtained the equation of order $O(\zeta^2)$ as follows:

$$\begin{aligned} \partial_0^2 u_2 + (2\partial_0\partial_2 + \partial_1^2)u_0 - d_0^2 u_2 - \cos(\theta + u_0)u_2 \\ - (2d_0 d_2 + d_1^2)u_0 = 2d_0 d_1 u_1 - 2\partial_0\partial_1 u_1. \end{aligned}$$

For $u_0 = 0$, the aforementioned equation will be,

$$\partial_0^2 u_2 - d_0^2 u_2 - \cos\theta u_2 = 2d_0 d_1 u_1 - 2\partial_0\partial_1 u_1. \tag{11}$$

Now using u_1 from equation (10), we obtain the following system of equations. The aforementioned system of equations for the region $X_0 < -a, |X_0| < a, X_0 > a$, respectively. Now substituting $u_2 = w_2(x)e^{i\eta t}$ in the aforementioned differential equation:

$$\begin{aligned} &\partial_0^2 w_2 - (1-\eta^2)w_2 \\ &\quad = 2\cos(a\sqrt{1+\eta^2})(i\eta d_1 E - \sqrt{1-\eta^2}\,\partial_1 E)e^{\sqrt{1-\eta^2}(a+X_0)}, \\ &\partial_0^2 w_2 + (1+\eta^2)w_2 \\ &\quad = 2[i\eta d_1 E\cos(X_0\sqrt{1+\eta^2}) \\ &\qquad + \sqrt{1+\eta^2}\,\partial_1 E\sin(X_0\sqrt{1+\eta^2})], \\ &\partial_0^2 w_2 - (1-\eta^2)w_2 \\ &\quad = 2\cos(a\sqrt{1+\eta^2})(i\eta d_1 E + \sqrt{1-\eta^2}\,\partial_1 E)e^{\sqrt{1-\eta^2}(a-X_0)}. \end{aligned}$$

These equations can be expressed with the help of an operator as follows:

$$L\psi = g(x).$$

Here, L is a self-adjoint and linear operator, *i.e.*, $(L = L^+)$. Also the periodic and smooth function $\ell : T \to \mathcal{R}$. Let the Hilbert space $\mathcal{L}^2(\mathcal{R})$ has the following inner product space

$$\langle f, h\rangle = \int_{-\infty}^{\infty} \overline{f}(\psi)h(\psi)\mathrm{d}\psi, \quad \forall f, h \in \mathcal{L}^2(\mathcal{R}).$$

Here, $\overline{f}(\psi)$ and $f(\psi)$ are the complex conjugate of each other. Now we have the in-homogeneous equation $L\phi = g(x)$. We can apply the Fredholm theorem, which gives sufficient and necessary conditions for the solution of such equation. So we obtained the following condition:

$$\int_{-\infty}^{\infty} Lg(x)d(x) = 0.$$

Now we apply the aforementioned result and obtained the following condition:

$$d_1 E = 0.$$

The required solution is given as follows:

$$u_2 = \partial_1 E e^{i\eta T_0}\begin{cases} C_{11}e^{\sqrt{1-\eta^2}X_0} & X_0 < -a, \\ \quad - X_0\cos(a\sqrt{1+\eta^2})e^{\sqrt{1-\eta^2}(a+X_0)} & \\ \quad + c.c, & \\ C_{12}\cos(X_0\sqrt{1+\eta^2}) & |X_0| \le a, \\ \quad + X_0\cos(X_0\sqrt{1+\eta^2}) + c.c, & \\ C_{13}e^{-\sqrt{1-\eta^2}X_0} & X_0 > a. \\ \quad - X_0\cos(a\sqrt{1+\eta^2})e^{\sqrt{1-\eta^2}(a-X_0)} & \\ \quad + c.c, & \end{cases}$$

Now by applying the continuity conditions at the discontinuity points, *i.e.*, $X_0 = \pm a$. The constants of integration $C_{11} = C_{12} = \cos(a\sqrt{1+\eta^2})$ and C_{13} are obtained. Note that $\partial_1 E$ as well as $\partial_n E$ in all calculations will not appear in the solvability conditions. Therefore, we assume the simple choice by

$$\partial_1 E = 0$$

also, if $\partial_1 E \neq 0$, then $(\zeta^2 u_2) > (\zeta u_1)$ as $X_0 \to \pm\infty$. The appearance of the term $(X_0 e^{\sqrt{1-\eta^2}(a\pm X_0)})$ in the aforementioned expression is leading to a nonuniformity in the perturbation expansion of u. The same procedure has been used in the study by Ali *et al.* [2].

2.1.4 $O(\zeta^3)$-equation

We obtained the equation of $O(\zeta^3)$ as follows:

$$\begin{aligned} O(\zeta^3): {} & \partial_0^2 u_3 + 2\partial_0\partial_1 u_2 + (2\partial_0\partial_3 + 2\partial_1\partial_2)u_0 + (2\partial_0\partial_2 + \partial_1^2)u_1 \\ & - d_0^2 u_3 - 2d_0 d_1 u_2 - (2d_0 d_3 + 2d_1 d_2)u_0 - (2d_0 d_2 + d_1^2)u_1 \\ & - \cos(\theta)u_3 - (2d_0^2)u_0 + \frac{1}{6}u_1^3\cos(\theta) = H\sin(\eta t). \end{aligned}$$

Rearranging the aforementioned equation and inserting the known values of u_0, u_1, and u_2, we obtain,

$$\begin{aligned} & \partial_0^2 u_3 - d_0^2 u_3 - \cos(\theta)u_3 \\ & = 2(d_0 d_2 - \partial_0\partial_2)u_1 + (d_1^2 - \partial_1^2)u_1 - \frac{1}{6}u_1^3\cos(\theta) - \frac{iH}{2} \end{aligned}$$

$$\partial_0^2 u_3 - d_0^2 u_3 - \cos(\theta)u_3 = \begin{cases} F_1, & X_0 < -a, \\ F_2, & |X_0| \le a, \\ F_3, & X_0 > a, \end{cases} \tag{12}$$

where F_1, F_2, and F_3 are given in Appendix A2.

The equations given in this Appendix are linear wave equations with forcing at frequencies η and 3η. As equation (12) is linear, so the solution can be written as a combination of the solutions with frequencies in terms of harmonics. The required forcing terms can be expressed as follows:

$$\begin{aligned} u_3 = {} & u_3^{(0)} + u_3^{(1)}e^{i\eta T_0} + c.c + u_3^{(2)}e^{2i\eta T_0} + c.c + u_3^{(3)}e^{3i\eta T_0} \\ & + c.c. \end{aligned} \tag{13}$$

Equation for the first Harmonic

We obtain an equation for the first harmonic:

$$\begin{aligned} & \partial_0^2 u_3^{(1)} - (1-\eta^2)u_3^{(1)} \\ & = \left[\frac{-iH}{2} + 2(i\eta d_2 E)\cos(a\sqrt{1+\eta^2})e^{\sqrt{1-\eta^2}(a+X_0)}\right. \\ & \quad \left. - \frac{1}{2}E|E|^2\cos^3(a\sqrt{1+\eta^2})e^{3\sqrt{1-\eta^2}(a+X_0)}\right] X_0 < -a, \\ & \partial_0^2 u_3^{(1)} + (1+\eta^2)u_3^{(1)} \\ & = \left[\frac{-iH}{2} + 2i\eta d_2 E\cos(X_0\sqrt{1+\eta^2})\right. \\ & \quad \left. + \frac{1}{2}E|E|^2\cos^3(X_0\sqrt{1+\eta^2})\right], \ |X_0| < a, \\ & \partial_0^2 u_3^{(1)} - (1-\eta^2)u_3^{(1)} \\ & = \left[\frac{-iH}{2} + 2(i\eta d_2 E)\cos(a\sqrt{1+\eta^2})e^{\sqrt{1-\eta^2}(a-X_0)}\right. \\ & \quad \left. - \frac{1}{2}E|E|^2\cos^3(a\sqrt{1+\eta^2})e^{3\sqrt{1-\eta^2}(a-X_0)}\right] X_0 > a. \end{aligned}$$

In the aforementioned equations, it should be noted that we have imposed $\partial_2 E = 0$ to obtain the equation for the first harmonic component, which gives us the solvability condition:

$$d_2 E = k_1 E|E|^2 i + L_1 H_1, \tag{14}$$

where

$$k_1 = \frac{\left(3 - 7\eta^4 - 2\eta^6 - 2\eta^2 + 6\sqrt{1-\eta^4}\tan^{-1}\left(\sqrt{\frac{1-\eta^2}{1+\eta^2}}\right)\right)}{32\eta\left(1 + \eta^2 + \sqrt{1-\eta^4}\tan^{-1}\left(\sqrt{\frac{1-\eta^2}{1+\eta^2}}\right)\right)} \quad (15)$$

and

$$L_1 = \frac{\eta\sqrt{1+\eta^2}}{\sqrt{2}\left(1 + \eta^2 + \sqrt{1-\eta^4}\tan^{-1}\left(\sqrt{\frac{1-\eta^2}{1+\eta^2}}\right)\right)}. \quad (16)$$

The numerical values of $k_1 = 0.0433270$ and $L_1 = -0.07339183$ for $\eta = 0.738$. The required solution for this harmonic can be obtained as follows:

$$u_3^{(1)} = \begin{cases} E|E|^2 v_1(X_0) + H\tilde{v}_1(X_0), & X_0 < -a, \\ E|E|^2 v_2(X_0) + H\tilde{v}_2, & |X_0| \le a, \\ E|E|^2 v_3(X_0) + H\tilde{v}_3(X_0), & X_0 > a. \end{cases}$$

Here, $v_1(X_0)$, $v_2(X_0)$, and $v_3(X_0)$ are defined in [2] and $\tilde{v}_1$, $\tilde{v}_2$, $\tilde{v}_3$ are given in the Appendix A3.

Analgously, $\aleph_1$, $\aleph_2$, and $\aleph_3$ are determined by applying the continuity conditions at the discontinuity points.

Equation for the third Harmonic

For third harmonic, we obtain the following system:

$$\partial_0^2 u_3^{(3)} - (\cos(\theta) - 9\eta^2)u_3^{(3)} = E^3\begin{cases} -\frac{1}{6}\cos^3(a\sqrt{1+\eta^2})e^{3\sqrt{1-\eta^2}(a+X_0)}, & X_0 < -a, \\ \frac{1}{6}\cos^3(X_0\sqrt{1+\eta^2}), & |X_0| \le a, \\ -\frac{1}{6}\cos^3(a\sqrt{1+\eta^2})e^{3\sqrt{1-\eta^2}(a-X_0)}, & X_0 > a. \end{cases}$$

By using the same procedure as for $u_3^{(1)}$, we obtained

$$u_3^{(3)}(X_0, T_0) = E^3\begin{cases} P_1(X_0), & X_0 < -a, \\ P_2(X_0), & |X_0| \le a, \\ P_3(X_0), & X_0 > a, \end{cases}$$

where P_1, P_2, and P_3 are defined in Appendix A4. Here, $\tilde{C}_1$, $\tilde{C}_2$, and $\tilde{C}_3$ are nonzero constants of integration that are also determined by the continuity conditions at the discontinuous points.

Note that due to the assumption $9\eta^2 > 0$, the second term in $P_1(X_0)$ and $P_3(X_0)$ will decay to zero. With the assumption $9\eta^2 > 0$, we see that $e^{3i\eta T_0}u_3^{(3)} + c.c.$ describes the left moving radiation for $X_0 < a$ and right moving radiation for $X_0 > a$, which are responsible for energy loss in the final equation.

2.1.5 $O(\zeta^4)$-equation

The equation for the $O(\zeta^4)$ as follows:

$$\begin{aligned}\partial_0^2 u_4 - d_0^2 u_4 + 2\partial_0\partial_1 u_3 + (2\partial_0\partial_2 + \partial_1^2)u_2 + (2\partial_0\partial_3 + 2\partial_1\partial_2)u_1 \\ + (2\partial_1\partial_3 + \partial_2^2)u_0 - 2d_0d_1u_3 - (2d_0d_2 + d_1^2)u_2 \\ - (2d_0d_3 + 2d_1d_2)u_1 \\ - (2d_1d_3 + d_2^2)u_0 - 2d_0^2 R u_1 = \cos(\theta + u_0)u_4.\end{aligned}$$

We substitute the values of u_1 and u_3 to obtain

$$\begin{aligned}\partial_0^2 u_4 - d_0^2 u_4 - \cos(\theta + u_0)u_4 \\ = 2(d_0d_1 - \partial_0\partial_1)u_3 + 2(d_1d_2 + d_0d_3)u_1 - 2(\partial_0\partial_3 + \partial_1\partial_2)u_1 \\ + 2d_0^2 R u_1.\end{aligned}$$

By using the solvability condition, we obtain $d_3E = -i\eta(ER)$ and $\partial_3 E = 0$. So we impose that $u_4(X_0, T_0) = 0$. This case is also similar to u_2. So we proceed to the next order of ζ.

2.1.6 $O(\zeta^5)$-equation

We obtain the following equation at $O(\zeta^5)$ as follows:

$$\begin{aligned}\partial_0^2 u_5 - d_0^2 u_5 + (2\partial_0\partial_2 + \partial_1^2)u_3 + (2\partial_0\partial_3 + 2\partial_1\partial_2)u_2 \\ + 2\partial_2\partial_3 u_0 + (2\partial_1\partial_3 + \partial_2^2)u_1 - (2d_0d_2 + d_1^2)u_3 \\ - (2d_0d_3 + 2d_1d_2)u_2 - 2d_2d_3u_0 + (2d_1d_3 + d_2^2)u_1 \\ - 4Rd_0d_1u_1 - 2Rd_0^2u_2 \\ = u_5\cos\theta + \left(-\frac{1}{2}u_1^2u_3 + \frac{1}{120}u_1^5\right)\cos\theta.\end{aligned}$$

By rearranging and inserting known values of u_0, u_1, u_2, u_3, and u_4 in the aforementioned differential equation, we obtain the following equation:

$$\begin{aligned}\partial_0^2 u_5 - d_0^2 u_5 - \cos(\theta)u_5 \\ = 2(d_0d_4 - \partial_0\partial_4)u_1 + 2(d_1d_3 - \partial_0\partial_3)u_1 + 2(d_2^2 - \partial_2^2)u_1 \\ + (d_1^2 - \partial_1^2)u_3 + 2(d_2d_0 - \partial_2\partial_0)u_3 \\ + \left(\frac{1}{2}u_1^2u_3 + + \frac{1}{120}u_1^5\right)\cos\theta.\end{aligned}$$

We use the known function and calculate the right-hand side to split the solution proportional to the simple harmonic. It is represented as follows:

$$\begin{aligned}u_5 = u_5^{(0)} + u_5^{(1)}e^{i\eta T_0} + c.c + u_5^{(2)}e^{2i\eta T_0} + c.c \\ + u_5^{(3)}e^{3i\eta T_0} + c.c. + u_5^{(4)}e^{4i\eta T_0} + c.c. + u_5^{(5)}e^{5i\eta T_0} + c.c.\end{aligned}$$

The equation for the first harmonic is given by

$$\partial_0^2 u_5^{(1)} - (\cos(\theta) - \eta^2)u_5^{(1)} = \begin{cases} G_1, & X_0 < -a, \\ G_2, & |X_0| \le a, \\ G_3, & X_0 > a, \end{cases} \quad (17)$$

where G_1, G_2, and G_3 are defined in Appendix A5 and $\upsilon_1(X_0)$, $\upsilon_2(X_0)$, and $\upsilon_3(X_0)$ are the bounded solution of $u_5^{(1)}(X_0, T_0)$ and $P_1(X_0)$, $P_2(X_0)$, and $P_3(X_0)$ are for $u_5^{(3)}(X_0, T_0)$ as solved earlier.

The solvability condition of Eq. (17) is given by

$$d_4E = k_2E|E|^4 + (L_2|E|^2 + L_3|E|^2)Hi. \tag{18}$$

Here, $k_2 = -(0.02741 + 0.0313811i)$, $L_2 = 0.027411 + 0.0313811i$, and $L_3 = 0.011147$. So far, we have obtained the leading-order behavior of the breathing amplitude from (14) and (18), which is our main objective in this work.

3 Amplitude equation

Now we defined an amplitude equation on the bases of the solvability conditions of each order of ζ. For the analytic approximation, we found the results up to order ζ^5. So the amplitude equation can be written as follows:

$$\left(\frac{\mathrm{d}E}{\mathrm{d}t}\right)_{O(\zeta^5)} = \zeta d_1E + \zeta^2 d_2E + \zeta^3 d_3E + \zeta^4 d_4E + O(\zeta^5). \tag{19}$$

By defining, $b = \zeta E$, $\Omega t = \eta\tau$, where b is the natural amplitude of the breathing mode. After these transformations, the aforementioned equation will gives us follows:

$$\frac{\Omega}{\eta}\frac{\mathrm{d}b}{\mathrm{d}t} = k_1b|b|^2i + L_1h - i\Omega\rho b + k_2b|b|^4 + L_2|b|^2h + L_3b^2h.$$

We obtain the final amplitude equation as follows:

$$\frac{\mathrm{d}b}{\mathrm{d}t} = \frac{\Omega}{\eta}(k_1b|b|^2i + L_1h - i\Omega\rho b + k_2b|b|^4 + L_2|b|^2h + L_3b^2h).$$

Here, we also follow Ali *et al.* [2]. The energy emission in terms of radiation decrease in the amplitude of oscillations. This satisfied the following form of radiation:

$$|b(t)| = \left[\frac{|b(0)|^4}{1 - 4\Re(\gamma)|b(0)t|}\right]^{1/4}. \tag{20}$$

Here, $\gamma = \Re(k_1) < 0$. This implies that modes decay algebraically. The decay rate is due to the assumptions taken in the third harmonics. Further, the nonlinearity is due to the formation of phonons that radiate energy to $x \to \pm\infty$.

4 Results and discussion of the analytic results

In this work, we study the parametric-driven sine-Gordon equation with phase shifts. For the numerical approximation, we use the Runge–Kutta method of order four (RK-4) with the help of Laplacian operator using a central difference discretization. For the numerical computation, we take the spatial and temporal discretization $\Delta x = 0.02$ and $\Delta t = 0.004$, respectively. Furthermore, the increasing damping at the boundaries during the periodic boundaries conditions is also considered.

The values of the constants are obtained in the aforementioned derivation with the help of MAPLE software. The values are given in Table 1.

The comparison of analytic and numerical solutions for the breathing modes of oscillation is shown in Figure 7. This clearly shows that the modes decay to a constant.

For the analytic solution, we used the multiple-scale expansion together with the perturbation method. For the perturbation method, we obtained the equations for the different order of the perturbed parameter ζ. For the stability, we checked the solution on each order of ζ. Moreover, we plotted the graphical representation of the breathing modes of $O(\zeta)$ in Figure 2 and for the $O(\zeta^2)$ in Figure 3. Also we discussed the various harmonics of $O(\zeta^3)$ and $O(\zeta^5)$. The plots of real and imaginary solutions of first harmonic in Figures 4 and 5. Figure 5 shows one of the interesting W-shape soliton solution, which was discussed in ref. [14]. It is observed in Figure 5 that the breathing mode is rapidly oscillating compared to the solution of order ζ^2. The rapid oscillatory behavior is due to the appearance of the driving terms in higher orders of ζ. This means that our driving term is approximated to order of ζ^3, *i.e.*, $h \sim O(\zeta^3)$. Due to this, the driving frequency appears in the higher order and oscillate the system rapidly.

Table 1: The numerical values of k's and L's with $\eta = 0.73825$

k's	L's
$k_1 = 0.04332700$	$L_1 = 0.07339183$
$k_2 = -(0.02741 + 0.0313811i)$	$L_2 = 0.027411 + 0.0313811i$
	$L_3 = 0.011147$

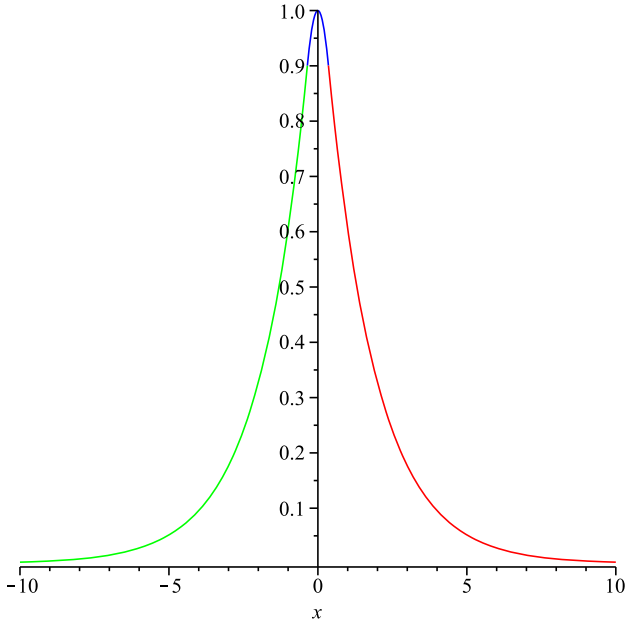

Figure 2: Breathing mode of $u_1(x, t)$ with $a = 0.4000012$ and $\eta = 0.73825$.

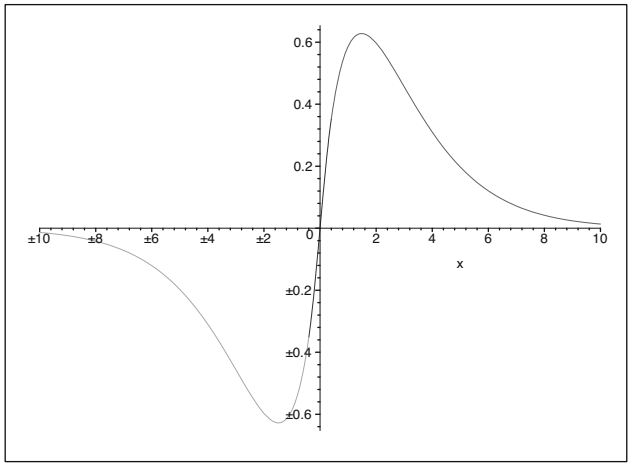

Figure 3: Breathing mode of $u_2(x, t)$ with $a = 0.4000012$ and $\eta = 0.73825$.

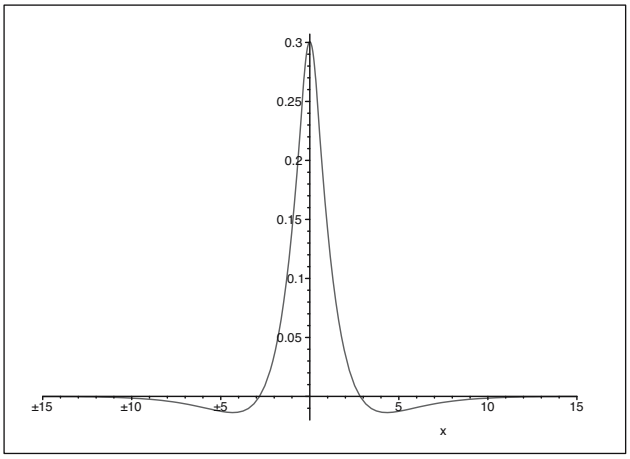

Figure 4: Breathing mode of $u_3^{(1)}$ imaginary solution with $a = 0.4$ and $\eta = 0.738$.

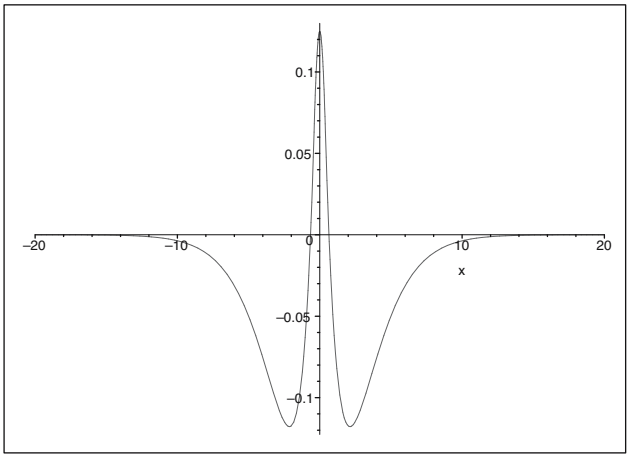

Figure 5: Breathing mode of $u_3^{(1)}$ imaginary solution with $a = 0.4$ and $\eta = 0.738$.

Furthermore, we discussed the driving case for the governing equation. In the driving case, the system oscillate and decay algebraically to a constant rate due to the presence of extra frequency and driving frequency terms. The derived numerical solution of the parametric sine-Gordon equation is also agreed with the analytical solution of amplitude equation as shown in Figure 7. Moreover, we tried to detect the resonance in the presence of external driving frequency when natural frequency is closed to driving frequency for the 0–π–0 junction. Hence, the multiple-scale expansions were used, and it was found that this resonating frequencies cannot excite the breathing mode if the amplitude is small enough. However, if the external drive amplitude is large enough, the junction can switch to the resistive state.

The solutions of the un-driven case has been plotted in Figure 6. It is observed in Figure 7 that the mode in the two junction types does not oscillate with an unbounded or growing amplitude. After a while, there is a balance of energy input into the breathing mode due to the external drive and the radiative damping. This result shows the regular oscillation of the mode that the junction voltage disappears even at the condition when the driving frequency is same as the eigen-frequency. This raises for the

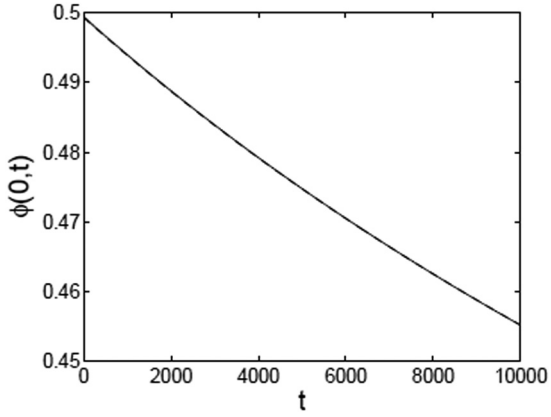

Figure 6: The comparison of un-driven case (*i.e.*, $h = 0$).

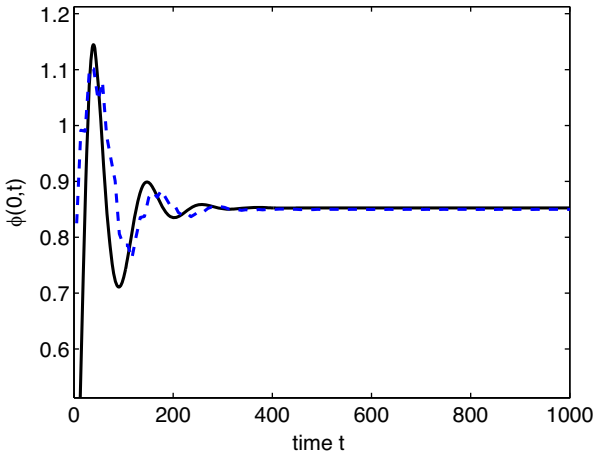

Figure 7: The comparison of analytical and numerical solutions of the driven case of the 0–π–0 junction with $h = 0.50$, and the dashed line denotes the numerical solution and solid shows analytic result, which shows the breathing mode of oscillation in parametric-driven sine-Gordon equation with phase shift.

question at which the breathing mode of a junction with a phase shift can be excited.

5 Conclusion

In this study, we considered in-homogeneous, nonlinear parametric-driven sine-Gordon equation with phase shifts, also known as nonlinear wave equation. This modeled an infinitely long Josephson junctions, driven by a microwave field. For the analytic solution, we constructed a perturbation series with multiple-scale expansion. For a small amplitude of oscillations, we discussed the breathing modes. We studied slowly varying amplitude of the oscillation for the 0–π–0 long Josephson junction. Further we obtained an amplitude equation which gives us an idea of the decay rate. In detail we studied the behavior of the breathing mode in different order of ζ. From that we observed that the system is oscillating more in higher order of ζ, while less in the lower order. Furthermore, we concluded that the modes decay to a constant. In future, we can increase the number of driven terms that can excite the defect mode of junction. We can also increase the driven frequencies for more rapid oscillation in a long Josephson Junction and other cases like 0–κ junction case.

Funding information: The authors extend their appreciation to the Deans of Scientific Research at King Khalid University, Abha, Saudi Arabia, for funding this work through research group program under grant number RGP-2-176-43.

Author contributions: All authors have accepted responsibility for the entire content of this manuscript and approved its submission.

Conflict of interest: The authors state no conflict of interest.

References

[1] Oxtoby OF, Barashenkov IV. Resonantly driven wobbling kinks. Phys Rev E. 2009;2:80.
[2] Ali A, Susanto H, Wattis JAD. Rapidly oscillating ac-driven long Josephson junctions with phase shifts. Phys D Nonlinear Phenom. 2013;246:15–22.
[3] Spagnolo B, Valenti D, Guarcello C, Carollo A, PersanoAdorno D, Spezia S, et al. Noise-induced effects in nonlinear relaxation of condensed matter systems. Chaos Solitons Fractals. 2015;81:412–24.
[4] Su SW, Gou SC, Liu IK, Bradley AS, Fialko O, Brand J. Oscillons in coupled Bose-Einstein condensates. Phys Rev A At Mol Opt Phys. 2015;91:1–9.
[5] Smirnov VV, Manevitch LI. The radial breathing mode in CNT - the nonlinear theory of the resonant energy exchange. Phys Rev B. 2015;1–8.
[6] Rossi JM. Non-Conservative variational approximation for nonlinear Schrödinger equations and its applications. PhD Dissertion, The Claremont Graduate University; 2016.
[7] Brito R, Cardoso V, Macedo CFB, Okawa H, Palenzuela C. Interaction between bosonic dark matter and stars. Phys Rev D Part Fields Gravit Cosmol. 2016;93(4):044045.
[8] Norma B-F, Cuauhtemoc C, Miguel C, Efrain R. Covariant approach of perturbations in Lovelock type brane gravity. Classical and Quantum Gravity. 2016;24(22):24501.
[9] Rehman S, Hussain A, Rahman JU, Anjum N, Munir T. Modified Laplace based variational iteration method for the mechanical

vibrations and its applications. Acta Mechanica et Automatica. 2022;16(2):98–104.
[10] Ahmad S, Ullah A, Akgül A, Jarad F. A hybrid analytical technique for solving nonlinear fractional order PDEs of power law kernel: Application to KdV and Fornberg-Witham equations. AIMS Math. 2022;7(5):9389–404.
[11] Pedder C, Meng T, Tiwari RP, Schmidt TL. Dynamic response functions and helical gaps in interacting Rashba nanowires with and without magnetic fields. Phys Rev B. 2016;54(24):1–5.
[12] Yin X, Radzihovsky L. Quench dynamics of spin-imbalanced Fermi-Hubbard model in one dimension. Phys Rev A. 2016;80309:1–31.
[13] Bambusi D, Maspero A. Freezing of energy of a Soliton in an external potential. Commun Math Phys. 2016;344:155–91.
[14] Wang L, Wang Z-Q, Zhang J-H, Qi F-H, Li M. Stationary nonlinear waves, superposition modes and modulational instability characteristics in the AB system. Nonlinear Dyn. 2016;86(1):185–96.
[15] Ahmad S, Susanto H, Wattis J. Existence and stability analysis of finite 0 − u − 0 Josephson junctions. Phys Rev B. 2009;80:1–9.
[16] Wright LG, Wabnitz S, Christodoulides DN, Wise FW. Ultrabroadband dispersive radiation by spatiotemporal oscillation of multimode waves. Phys Rev Lett. 2015;115:1–5.
[17] Ali A, Susanto H, Wattis JAD. Decay of bound states in a sine-Gordon equation with double-well potentials. J Math Phys. 2015;56(5):50–65.
[18] She XW, Ni QQ, Shi JX, Natsuki T. Radial breathing mode of carbon nanotubes subjected to axial pressure. Nanoscale Res Lett. 2011;6(1):1–6.
[19] Strozzi M, Smirnov VV, Manevitch LI, Pellicano F. Nonlinear vibrations and energy exchange of single-walled carbon nanotubes. Radial breathing modes. Composite Struct. 2015;184:613–32.
[20] Araujo PT, Fish PBC, Dresselhaus MS, Sato K, Saito R, Jorio A. Resonance Raman spectroscopy of the radial breathing modes in carbon nanotubes. Physica E. 2010;42:1251–61.
[21] Batra RC, Gupta SS. Wall thickness and radial breathing modes of single-walled carbon nanotubes. J Appl Mech. 2008;75(6):610–8.

Appendix

A.1 Order u_2

$$\begin{aligned}
\partial_0^2 u_2 - d_0^2 u_2 - u_2 &= 2\cos(a\sqrt{1+\eta^2})(i\eta d_1 E - \sqrt{1-\eta^2}\,\partial_1 E) \\
&\quad \times e^{\sqrt{1-\eta^2}(a+X_0)+i\eta T_0} + c.c, \\
\partial_0^2 u_2 - d_0^2 u_2 + u_2 &= 2[i\eta d_1 E\cos(X_0\sqrt{1+\eta^2}) \\
&\quad + \sqrt{1+\eta^2}\,\partial_1 E\sin(X_0\sqrt{1+\eta^2})]e^{i\eta T_0} + c.c, \\
\partial_0^2 u_2 - d_0^2 u_2 - u_2 &= 2\cos(a\sqrt{1+\eta^2})(i\eta d_1 E + \sqrt{1-\eta^2}\,\partial_1 E) \\
&\quad \times e^{\sqrt{1-\eta^2}(a-X_0)+i\eta T_0} + c.c.
\end{aligned}$$

A.2 Order u_3

$$\begin{aligned}
F_1 = \Big[&- \frac{iH}{2} + 2(i\eta d_2 E \\
&- \sqrt{1-\eta^2}\,\partial_2 E)\cos(a\sqrt{1+\eta^2})e^{\sqrt{1-\eta^2}(a+X_0)} \\
&- \frac{1}{2}E|E|^2\cos^3(a\sqrt{1+\eta^2})e^{3\sqrt{1-\eta^2}(a+X_0)}\Big]e^{i\eta T_0} + c.c \\
&- \frac{1}{6}E^3\cos^3(a\sqrt{1+\eta^2})e^{3\sqrt{1-\eta^2}(a+X_0)+3i\eta T_0},
\end{aligned}$$

$$\begin{aligned}
F_2 = \Big[&- \frac{iH}{2} + 2i\eta d_2 E\cos(X_0\sqrt{1+\eta^2}) \\
&+ 2\partial_2 E\sqrt{1+\eta^2}\sin(X_0\sqrt{1+\eta^2}) \\
&+ \frac{1}{2}E|E|^2\cos^3(X_0\sqrt{1+\eta^2})\Big]e^{i\eta T_0} \\
&+ \frac{1}{6}E^3\cos^3(X_0\sqrt{1+\eta^2})e^{3i\eta T_0}
\end{aligned}$$

$$\begin{aligned}
F_3 = \Big[&- \frac{iH}{2} + 2(i\eta d_2 E \\
&+ \sqrt{1-\eta^2}\,\partial_2 E)\cos(a\sqrt{1+\eta^2})e^{\sqrt{1-\eta^2}(a-X_0)} \\
&- \frac{1}{2}E|E|^2\cos^3(a\sqrt{1+\eta^2})e^{3\sqrt{1-\eta^2}(a-X_0)}\Big]e^{i\eta T_0} \\
&- \frac{1}{6}E^3\cos^3(a\sqrt{1+\eta^2})e^{3\sqrt{1-\eta^2}(a-X_0)+3i\eta T_0}.
\end{aligned}$$

A.3 Order u_3, first harmonic

$$\begin{aligned}
\tilde{v}_1(X_0) &= \aleph_1 e^{\sqrt{1-\eta^2}X_0} \\
&\quad + \frac{\left(1+2\left(\sqrt{1-\eta^2}X_0 - \frac{1}{2}\right)L_1\eta\right)}{-2+2\eta^2} \\
&\quad \times \frac{\cos(\sqrt{1+\eta^2}\,a)e^{\sqrt{1-\eta^2}(a+X_0)})}{-2+2\eta^2}
\end{aligned}$$

$$\begin{aligned}
\tilde{v}_2(X_0) &= \aleph_2\cos(\sqrt{1+\eta^2}X_0) \\
&\quad - \frac{(\eta L_1 X_0(1+\eta^2)\sin(\sqrt{1+\eta^2}X_0))}{(1+\eta^2)^{\frac{3}{2}}} \\
&\quad + \frac{\sqrt{1+\eta^2}\left(\eta L_1\cos(\sqrt{1+\eta^2}X_0) - \frac{1}{2}\right)}{(1+\eta^2)^{\frac{3}{2}}},
\end{aligned}$$

$$\begin{aligned}
\tilde{v}_3(X_0) &= \aleph_3 e^{-\sqrt{1-\eta^2}X_0} + \frac{\left(1+2\left(\sqrt{1-\eta^2}X_0 - \frac{1}{2}\right)L_1\eta\right)}{-2+2\eta^2} \\
&\quad \times \frac{\cos(\sqrt{1+\eta^2}\,a)e^{\sqrt{1-\eta^2}(a-X_0)})}{-2+2\eta^2}.
\end{aligned}$$

A.4 Order u_3 third harmonic

$$P_1(X_0) = \tilde{C}_1 e^{\sqrt{1-9\eta^2}X_0} - \frac{1}{48}\cos^3(a\sqrt{1+\eta^2})e^{3\sqrt{1-\eta^2}(a+X_0)},$$

$$P_2(X_0) = \tilde{C}_2\cos(X_0\sqrt{1+9\eta^2}) - \frac{1}{192\eta^2}(\eta^2-3)\cos(X_0\sqrt{1+\eta^2}),$$

$$P_3(X_0) = \tilde{C}_3 e^{-\sqrt{1-9\eta^2}X_0} - \frac{1}{48}\cos^3(a\sqrt{1+\eta^2})e^{3\sqrt{1-\eta^2}(a-X_0)}.$$

A.5 Order u_5 first harmonic

$$\begin{aligned} G_1 = {} & (2i\eta d_4 E - k_1 E|E|^4 - k_1 L_1 |E|^2 H) \\ & \times \cos(a\sqrt{1+\eta^2})e^{\sqrt{1-\eta^2}(a+X_0)} \\ & - 2\eta(k_1 E|E|^4 + L_1 H|E|^2)\upsilon_1(X_0) \\ & - \frac{1}{2}E|E|^4\cos(a\sqrt{1+\eta^2})e^{\sqrt{1-\eta^2}(a+X_0)}(3\upsilon_1(X_0)) \\ & + P_1(X_0) + \frac{1}{12}E|E|^4\cos^5(a\sqrt{1+\eta^2})e^{5\sqrt{1-\eta^2}(a+X_0)} \\ & - \left(\frac{1}{2}E^2 + |E|^2\right)H\cos^2(a\sqrt{1+\eta^2})e^{\sqrt{1-\eta^2}(a+X_0)}\tilde{\upsilon}_1(X_0), \end{aligned}$$

$$\begin{aligned} G_2 = {} & (2i\eta d_4 E - k_1 E|E|^4 - k_1 L_1 |E|^2 H)\cos(X_0\sqrt{1+\eta^2}) \\ & - 2\eta(k_1 E|E|^4 + L_1 H|E|^2)\upsilon_2(X_0) \\ & + \frac{1}{2}E|E|^4\cos^2(X_0\sqrt{1+\eta^2})(3\upsilon_2(X_0) + P_2(X_0)) \\ & - \frac{1}{12}E|E|^4\cos^5(X_0\sqrt{1+\eta^2}) \\ & + \left(\frac{1}{2}E^2 + |E|^2\right)H\cos^2(X_0\sqrt{1+\eta^2})\tilde{\upsilon}_2(X_0), \end{aligned}$$

$$\begin{aligned} G_3 = {} & (2i\eta d_4 E - k_1 E|E|^4 - k_1 L_1 |E|^2 H) \\ & \times \cos(a\sqrt{1+\eta^2})e^{\sqrt{1-\eta^2}(a-X_0)} \\ & - 2\eta(k_1 E|E|^4 + L_1 H|E|^2)\upsilon_3(X_0) - \frac{1}{2}E|E|^4 \\ & \times \cos(a\sqrt{1+\eta^2})e^{\sqrt{1-\eta^2}(a-X_0)}(3\upsilon_3(X_0)) \\ & + P_3(X_0) + \frac{1}{12}E|E|^4\cos^5(a\sqrt{1+\eta^2})e^{5\sqrt{1-\eta^2}(a-X_0)} \\ & - \left(\frac{1}{2}E^2 + |E|^2\right)H\cos^2(a\sqrt{1+\eta^2})e^{\sqrt{1-\eta^2}(a-X_0)}\tilde{\upsilon}_3(X_0). \end{aligned}$$